A Level Set Method for Gland Segmentation

Chen Wang[1], Hong Bu[2], Ji Bao[2], and Chunming Li[1]
University of Electronic Science and Technology of China[1], Sichuan University[2]
cmli@ieee.org

Abstract

Histopathology plays a role as the gold standard in clinic for disease diagnosis. The identification and segmentation of histological structures are the prerequisite to disease diagnosis. With the advent of digital pathology, researchers' attention is attracted by the analysis of digital pathology images. In order to relieve the workload on pathologists, a robust segmentation method is needed in clinic for computer-assisted diagnosis. In this paper, we propose a level set framework to achieve gland image segmentation. The input image is divided into two parts, which contain glands with lumens and glands without lumens, respectively. Our experiments are performed on the clinical datasets of West China Hospital, Sichuan University. The experimental results show that our method can deal with glands without lumens, thus can obtain a better performance.

1. Introduction

Histopathology is the study of signs of disease using the microscopic examination of a biopsy or surgical specimen that is processed and fixed onto glass slides [4]. To reveal the components of tissue and structures of interest, Hematoxylin-Eosin (H&E) staining has been used by pathologists for over a hundred years. Now the H&E stained image is still widely used in clinic and plays a central role in diagnosis. The reason why histopathology attracts the researchers' attentions is that it plays a role as the gold standard in clinic for diagnosing considerable number of diseases.

With the advent and development of digital pathology, the research of automatic histopathology image analysis attracts interest of many researchers. In this paper, we focus on the analysis of the endometrial gland H&E stained images used in clinic. Pathologists distinguish the glandular structure from three major structures in the endometrial gland H&E stained image, which are vessels, glands and stromal nuclei, as Fig. 1(a) shows. The primary concern of pathologists in clinic is the area of the epithelial layers of glands and stromal nuclei. In order to accomplish this,

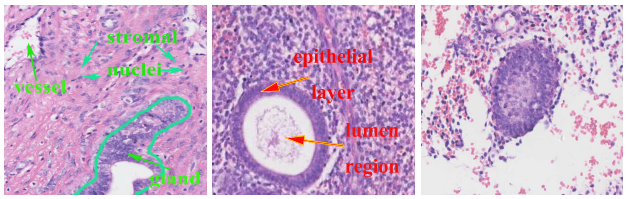

(a) (b) (c)

Figure 1. Illustration of the morphology of glands in an H&E stained image. Fig. (a) shows the major structures in a gland image. Fig. (b) shows the glandular structure with a lumen and Fig. (c) shows the glandular structure without a lumen. Note that every gland has its lumen but may not show in an H&E stained image.

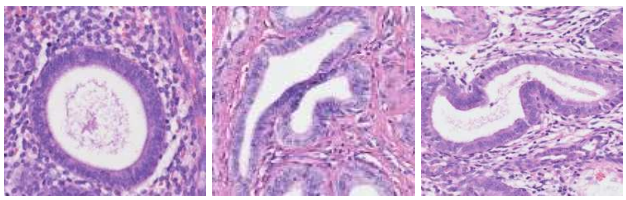

Figure 2. Shape variety of endometrial glands.

pathologists require to distinguish glands and stromal nuclei from other structures, and count their areas, respectively. Thus gland segmentation is a key problem for diagnosis.

Fig. 1(b) shows the common glandular structure, which is familiar to most algorithm researchers without the medical background. These common glands in the H&E stained image comprise lumens and epithelial layers. We can observe that lumens are surrounded by epithelial layers. However, Fig. 1(b) is not the only structural form of the gland in the H&E stained image. In the process of making tissue slice, the pathologist may cut the margin of the gland which the lumen is not included. As a result, there are several glands containing only epithelial layers in the H&E stained image, as Fig. 1(c) shows. We call these glandular structures as glands without lumens in this paper. It is worth mentioning that they also contain lumens but the lumens can not be observed in the image.

Many algorithms have been used for gland segmenta-

tion in recent years. For example, popular deep learning methods have been applied [2][5]. Chen et al.[2] proposed an efficient deep contour-aware network (DCAN) under a unified multi-task learning framework. The advantage of deep learning method is its reliable results. However, the training process of deep learning method needs considerable numbers of manual-labeled training images, which are difficult and expensive to obtain. Moreover, a well trained deep learning model may need enormous time to be trained, and the trained deep learning model using one kind of specific gland images may not suitable for other kinds of gland images.

Besides, a popular scheme for gland segmentation combines classification and level set method [4]. In this scheme, we need to train a classifier first for recognizing the nuclei. Then structural constraints are used to reduce the number of false positive regions. Finally we initialize a level set with an energy defined based on Bayesian probability scene. Naik et al.[8] proposed an automated segmentation method in this scheme using low level and high level information.

In addition, model-based and structure-based methods are proposed using the prior of the glandular structure [3][9][10]. Through modeling the regular glandular structures, Cigdem et al.[3] proposed an object-graph approach which achieves acceptable performance on the circular glands. However, since focusing on the circular glands, the method fails to deal with the shape variety of glands (Fig. 2). Nguyen et al. [9] proposed a segmentation algorithm using structural and contextual information. By associating nuclear objects with the lumen objects, it can achieve acceptable performance. But it can not deal with glands without lumens.

There are two factors making the gland segmentation a tough problem. Due to the shape variety of glands, different staining degree of H&E stained images and numerous glands in one image, it is difficult to design a robust algorithm to conquer the field. Additionally, there are glands without lumens in the H&E stained image. Many algorithms such as [9] cease to be effective when dealing with these glandular structures.

In this paper, we propose to obtain different glandular structures (i.e., glands with and without lumens). To achieve this purpose, we build a novel level set framework in which two level sets defined in different models are used for different glandular structures. One level set is designed for the glands with lumens and the other is designed for the glands without lumens. The experimental results show that our method can obtain both two glandular structures, and achieve better performance.

2. The framework of gland segmentation

According to the pathology knowledge described in section 1, we consider the whole H&E stained image as two parts. The one contains the glands with lumens and the other is the rest region of the whole image which may contain glands without lumens or no gland. In this paper, we call these two parts as the main part and the complementary part respectively because the former part contains most glands in the whole image and the latter part is used for searching the gland without lumens which can't be located by lumens. The main part and complementary part are illustrated in Fig. 3, which can be achieved by the following two steps. First the main part is located by the guide of the order of arrangement of glandular structure that lumens are surrounded by their epithelial layers. Then we regard the rest region as the complementary part.

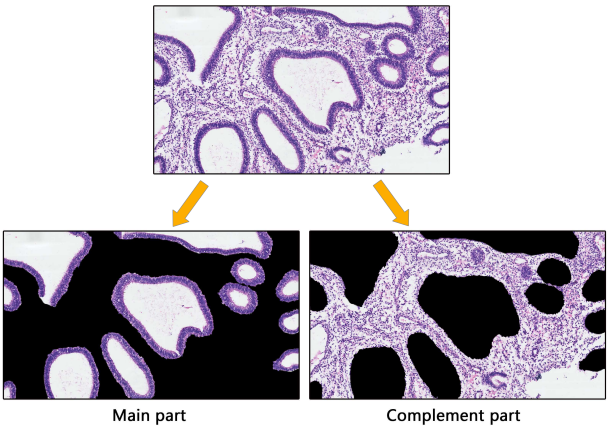

Figure 3. Illustration of the main part and complementary part

We can observe that the lumen regions are always white or mostly white regardless of the staining degree of the H&E stained image. Thus, the white regions can be easily obtained, as Fig. 5(a) shows. See section 3.1, a level set is introduced for the region. However, the vessels are also white, which can be obtained by the above algorithm applied for the lumen region. Hence, the first step needs an additional operation to remove the interference of vessels (see section 3). After the removing vessel process, we can locate the lumen regions, as Fig. 5(c) shows. Following the localization operation, we want to obtain the regions of glands with lumens as the foregoing statement. The method for the corresponding epithelial layers is described in section 3. We use the 0, k level sets to represent the boundaries of the lumens and epithelial layers, respectively. So the regions surrounded by the k level set can be regarded as the main part, as Fig. 4(b) shows. The rest part outside the k level set is considered as the complementary part.

As the foregoing statement, the complementary part may contain glands without lumens or no gland. What we want is to catch the rest glands if there are glands without lumens remained in the complementary part. Note that glands without lumens consist of only epithelial layers and the shape of them is nearly circular. We utilize the above prior knowl-

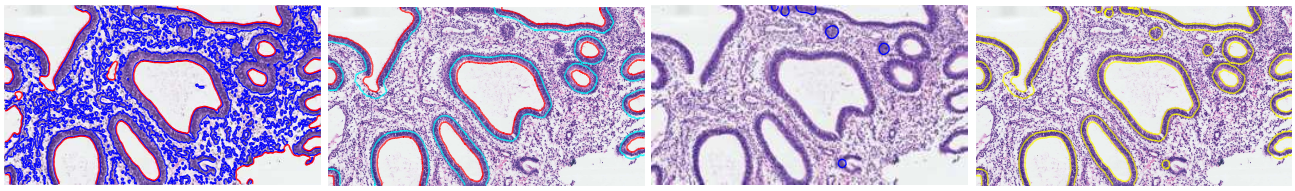

(a) The contours represented by the zero level of two level sets: ϕ_1 in red and ϕ_2 in blue.

(b) The main part inner the k level of ϕ_1 (cyan). The rest part outside the k level set is the complementary part.

(c) Obtained glands in the complementary part

(d) The result that combines obtained glands in the main part and the complementary part

Figure 4. The illustration of our method. See text for explanation.

edge to locate them by the distribution of the cell nuclei. The detailed method is described in section 3.

3. Method

In this section, our proposed level set framework is introduced for image segmentation of the corresponding glandular regions in the main part and the complementary part. In our level set framework, two different level sets are used to segment the lumen regions and the epithelial layer regions respectively. Note that, according to section 2, the main part is obtained when the segmentation of glands with lumens has finished. The whole process of our method is illustrated in Fig. 4.

Our method consists of three steps designed following the statement in section 2. Firstly, two level sets defined in edge-based model and region-based model respectively are initialized and evolved simultaneously. The former level set is used for locating the lumen regions, and the latter level set is used for obtaining the epithelial layers, which contains both the epithelial layers of glands with or without lumens. As shown in Fig. 4(a), The regions represented by the two level sets don't overlap because of the mutual exclusion constraint term in our method. Then, the vessel regions are removed so the former level set locates only lumen regions. Represented by the k level of the former level set, the epithelial layers of the located lumens are obtained. As Fig. 4(b) shows, the main part is the regions surrounded by the k level of the former level set (contour in cyan), and the rest region is the complementary part. Note that, the epithelial layers represented by the former level set using the location of lumen regions are also included in the latter level set which focuses on the epithelial layers. In the last step, the latter level set needs only to search the glands without lumens in the complementary part. The result shown in Fig. 4(c) can be obtained after searching in the remaining epithelial layers in the complementary part. As Fig. 4(d) shows, the final segmentation result is the regions represented by the combination of two level sets.

3.1. Level set framework and energy functional

The segmentation under a level set framework is achieved by looking for a level set function which minimizes an energy functional. The energy functional can be defined specifically according to the certain application. The process of level set method starts from initializing a level set. Then the level set evolves according to the evolution equation until the zero level set reaches to the desired boundaries. Similarly but beyond the original model, two level sets are used simultaneously to achieve the image segmentation in our proposed framework. One level set, denoted as ϕ_1, is defined for the localization of the lumen regions and the segmentation of the glands with lumens. The other, denoted as ϕ_2, plays the role in segmenting the possibly existed glands without lumens in the complementary part. The energy functional is defined as follows:

$$E(\phi_1, \phi_2, f_1, f_2) = E_1(\phi_1) + E_2(\phi_2, f_1, f_2) + P(\phi_1, \phi_2) \quad (1)$$

where $E_1(\phi_1)$ and $E_2(\phi_2, f_1, f_2)$ are the energy functionals defined for each level set according to different models; And $P(\phi_1, \phi_2)$ is the mutual exclusion constraint term, which forces the level set functions to segment the nonoverlapping regions.

The level set ϕ_1, which plays a role in segmenting the glands with lumens, is defined in an edge-based model. Specifically, we use the DRLSE model for the reference to define the corresponding energy functional [7].

$$E_1(\phi_1) = R_p(\phi_1) + L_g(\phi_1) + A_g(\phi_1) \quad (2)$$

where $R_p(\phi_1)$ is the distance regularization term which keeps the regularity of level set; $L_g(\phi_1)$ and $A_g(\phi_1)$ are data terms which are introduced in the following paragraph.

The difference between the level set in our framework and DRLSE model is that we use the 0, k level of ϕ_1 to obtain the boundaries of lumen regions and the corresponding epithelial layers, respectively. In our framework, we continue to use the distance regularization term in DRLSE model since the regularity of level set should be kept so that

no re-initialization is needed.

$$R_p(\phi_1) = \mu_1 \int \frac{1}{2}(|\nabla\phi_1(x)| - 1)^2 dx \quad (3)$$

where μ_1 is the coefficient and ∇ represents the gradient operator.

The difference can be seen in data terms, which are defined as follows.

$$L_g(\phi_1) = \int g[\lambda_{1,0}\delta(\phi_1) + \lambda_{1,k}\delta(\phi_1 - k)]|\nabla\phi_1|dx \quad (4)$$

$$A_g(\phi_1) = \int \alpha_{1,0}\, gH(-\phi_1) + \alpha_{1,k}\, gH(-\phi_1 + k)dx \quad (5)$$

where $\lambda_{1,0}$, $\lambda_{1,k}$, $\alpha_{1,0}$ and $\alpha_{1,k}$ are corresponding coefficients. H and δ are the Heaviside function and Dirac function, respectively. g in formula (4) is the edge indicator function defined as:

$$g = \frac{1}{1 + |\nabla G_\sigma * I|^2} \quad (6)$$

where G_σ is the Gaussian kernel with a standard deviation σ.

To deal with H&E stained images, our model is fit for color images by taking three channels into account. Similar to the gray image, the boundaries in color image can also be indicated by the high gradient magnitude computed by three channels. So the edge-based model achieves the segmentation by moving the contours towards the desired boundaries on which we can capture by high gradient magnitude. The role which L_g plays is to drive the contours towards the boundaries with a high gradient magnitude. And the weighted area term A_g plays a role in speeding up the evolution when the contour is far from the desired boundaries.

The level set ϕ_2, which plays a role in searching and segmenting the possibly existed glands without lumens, is defined in a region-based model. Different from the edge-based model, the region-based model utilizes the color information, which can capture the certain region with the similar color. We use the RSF model for reference to define the following energy functional in our method [6].

$$E_2(\phi_2, f_1, f_2) = R(\phi_2) + D(\phi_2, f_1, f_2) + A_l(\phi_2) \quad (7)$$

where R has the same function as R_p in formula (3). D is the data term which specifies the function of region-based model that is to obtain the region with the similar color. A_l is the arc length term which smooths the contour represented by zero level set through minimizing the arc length of the contour.

$$R(\phi_2) = \mu_2 \int \frac{1}{2}(|\nabla\phi_2(x)| - 1)^2 dx \quad (8)$$

$$A_l(\phi_2) = \nu_2 \int |\nabla H(\phi_2(x))|dx \quad (9)$$

$$D(\phi_2) = \sum_{i=1}^{2} \lambda_{2,i} \int \left(\int K_\sigma(y - x)|I(y) - f_i(x)|^2 M_i(\phi_2(y))dy \right) dx \quad (10)$$

where K_σ is a nonnegative kernel function with a localization property [6]. f_1 and f_2 are two values that approximate image colors. $M_i(\phi_2)$ is the membership function which can be defined as $M_1(\phi_2) = H(\phi_2)$ and $M_2(\phi_2) = 1 - H(\phi_2)$.

In our proposed framework, the mutual exclusion constraint term plays a vital role in keeping our method which consists of two level sets from obtaining the overlapping regions so that the segmentation results are consistent. To achieve this purpose, we define the following energy functional.

$$P(\phi_1, \phi_2) = \gamma \int H(-\phi_1)H(-\phi_2)dx \quad (11)$$

where γ is the coefficient of the energy $P(\phi_1, \phi_2)$. When the regions represented by two level sets ϕ_1 and ϕ_2 don't overlap, the energy functional $P(\phi_1, \phi_2)$ reaches its minimum.

3.2. Energy minimization

The desired level set with its 0, k levels representing the evolved contours of the objects is the level set which minimizes an energy functional. Hence, we need to minimize the energy functional (1). According to the calculus of variations [1], we can minimize the energy functional $F(\phi)$ by the gradient flow equation:

$$\frac{\partial\phi}{\partial t} = -\frac{\partial F}{\partial\phi} \quad (12)$$

where $\frac{\partial F}{\partial\phi}$ is the Gâteaux derivative of the functional F. This evolution equation indicates the level set to evolve towards the opposite direction of the Gâteaux derivative(i.e., the gradient descent direction). In our framework, the two level sets are evolved simultaneously but the gradient flow equations are calculated differently and separately.

We need to calculate the Gâteaux derivative $\frac{\partial}{\partial\phi_1}E(\phi_1, \phi_2, f_1, f_2)$, $\frac{\partial}{\partial\phi_2}E(\phi_1, \phi_2, f_1, f_2)$ for each level set individually. The corresponding energy functional $E(\phi_1, \phi_2)$ for the level set ϕ_1 can be minimized by solving

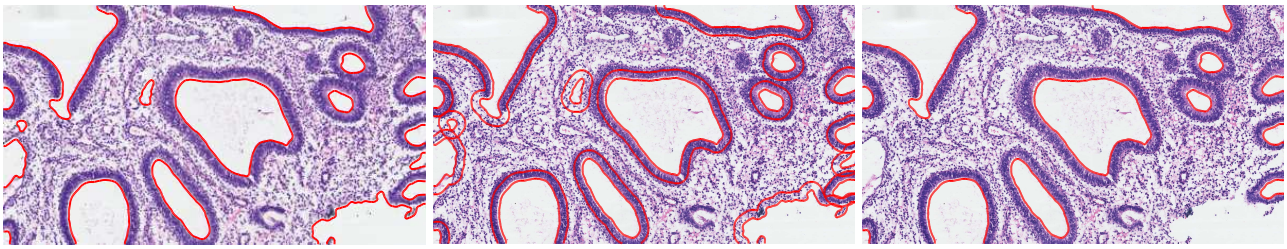

(a) The white part represented by the zero level of ϕ_1 (b) The surrounding regions of the white part (c) The lumen regions after removing the vessels

Figure 5. The process of removing vessels from the white regions.

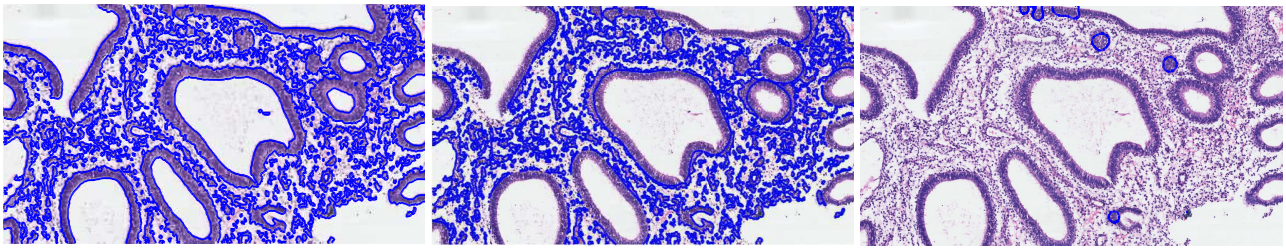

(a) (b) (c)

Figure 6. The process of searching the glands without lumens. Fig. (a) shows the epithelial layers represented by the zero level of ϕ_2. Note that it contains the epithelial layers which has been obtained in ϕ_1. Fig. (b) shows the epithelial layers in the complementary part of ϕ_2. Fig. (c) is the obtained glands without lumens.

the following gradient flow:

$$\frac{\partial \phi_1}{\partial t} = [\lambda_{1,0}\delta(\phi_1) + \lambda_{1,k}\delta(\phi_1 - k)]div\left(g\frac{\nabla\phi_1}{|\nabla\phi_1|}\right) + \alpha_{1,0}g\delta(\phi_1) + \alpha_{1,k}g\delta(\phi_1 - k) + \gamma\delta(-\phi_1)H(\phi_2) + \mu_1\left[\nabla^2\phi_1 - div\left(\frac{\nabla\phi_1}{|\nabla\phi_1|}\right)\right] \tag{13}$$

where $div(\cdot)$ is the divergence operator.

As for the level set ϕ_2 which defined in a region-based model, we need to calculate ϕ_1, f_1 and f_2 in order to let the energy functional $E(\phi_1, \phi_2, f_1, f_2)$ reach its minimum. The process is as follows: for a fixed level set function ϕ_2, we minimize $E(\phi_1, \phi_2, f_1, f_2)$ with respect to f_1 and f_2 which can be calculated as:

$$f_i(x) = \frac{K_\sigma * [M_i(\phi_2(x))I(x)]}{K_\sigma * M_i(\phi_2(x))}, i = 1, 2 \tag{14}$$

Then, for fixed f_1 and f_2, we minimize $E(\phi_1, \phi_2, f_1, f_2)$ with respect to ϕ_2, which can be done by solving the following gradient flow:

$$\frac{\partial \phi_2}{\partial t} = -\delta(\phi_2)(\lambda_{2,1}e_1 - \lambda_{2,2}e_2) + \nu_2\delta(\phi_2)div\left(\frac{\nabla\phi_2}{|\nabla\phi_2|}\right) + \mu_2\left(\nabla^2\phi_2 - div\left(\frac{\nabla\phi_2}{|\nabla\phi_2|}\right)\right) + \gamma\delta(-\phi_2)H(\phi_1) \tag{15}$$

where $e_i(x) = \int K_\sigma(y-x)|I(x) - f_i(y)|^2 dy,\ i = 1, 2$ and $f_i(x)$ is the formula (14).

In our proposed method, two level sets play a vital role in image segmentation. But two operations are also needed according to the previous statement.

Removing vessels As the foregoing statement, the white region represented by the zero level of ϕ_1 in the first step contains both the vessels and lumens, as Fig. 5(a) shows. Hence, the first step needs an additional operation to remove the interference of vessels. Note that the morphology difference between lumens and vessels is whether the white regions have epithelial layers or not. We calculate the ratio of the nuclear areas in the surrounding regions as the criterion for distinguishing these two structures.

As Fig. 5(b) shows, the surrounding regions can be obtained simply by extending the white region to a proper size. Each surrounding region is invited for calculation and judgement individually. During the distinguishing process for any surrounding region, the area of surrounding region is calculated as the area between 0 and k levels (see section 3.1); And the area of the cell nuclei can be calculated by counting the pixels of nuclei after applying a clustering algorithm. Once the ratio is calculated, the region with a high ratio will be recognized as the glandular epithelial layer and the white region surrounded by this epithelial layer is preserved. The result after removing vessels is shown in Fig. 5(c).

Searching for the glands without lumens The level set ϕ_2 is introduced for the candidate epithelial layers of glands without lumens. As Fig. 6(a) shows, all the epithelial layers of glands with or without lumens and stromal nuclei are obtained after the iteration of ϕ_2. However, we need only to search the epithelial layers in the complementary part since those epithelial layers of glands with lumens are represented by the k level of ϕ_1. Hence in the last step, when the main part and the complementary part are obtained, we search the complementary part to find out whether there are glands without lumens. We can simply search the epithelial layers in the complementary part represented by the zero level of ϕ_2, as Fig. 6(b) shows.

It is quite clear that the glands without lumens consist of only epithelial layers and the shape of them is nearly circular, while the stromal nuclei have a scattered distribution. Several stromal nuclei clusters form an irregular shape. Observed that, we constrain the regularity of ϕ_2 and the smoothness of the zero level of ϕ_2. The contour of stromal nuclei shrinks during the iteration of the level set and disappear finally. The epithelial layers of glands can be kept because of their regular shapes. The result is shown in Fig. 6(c).

4. Implementation and experimental results

Our experimental H&E stained images are obtained from West China Hospital, Sichuan University, which are the clinical data of endometrial glands. The dataset consists of 18 H&E stained images and the corresponding segmentation ground truth.

4.1. Pre-processing

Image analysis scientists are trying to come to terms with the enormous density of data that histopathology holds [4]. In our endometrial gland segmentation, the original H&E stained images are high-resolution which comprise approximately 2000×3000 spatial elements. The high-resolution images bring two major problems which seriously influence the image segmentation process. Since the size of the image is enormous, the calculation is time consuming. As a result, the evolution of the level set is slow. In addition, the segmentation algorithm tends to obtain the detailed nuclear regions under the high-resolution image. For our proposed approach, if we evolved the level set under the high-resolution image, the results would be the nuclear boundaries.

In order to facilitate the image segmentation and weaken the influence of the high-resolution, we apply the down sampling and smoothing operation as pre-processing. However, if we down sampled the original image to an overly small size, it would damage the clarity of the image. Hence, considered the trade-off between the consuming time and the size and clarity of the processing image according to the need of applied algorithm, we down sample each image as $1/8$ of the original size, and the optional smoothing is performed before down sampling.

To prove the rationality of pre-processing, we are willing to mention that the algorithm [9] used for comparison also suffers from high-resolution images, which cause it to obtain the detailed structures such as nuclei and slow the speed of algorithm violently. Our pre-processing can help it to achieve higher performance and also accelerate dramatically.

4.2. Implementation details

In practice, the Heaviside function $H(\phi)$ and Dirac delta function $\delta(\phi)$ in the above energy functionals are approximated by the following smooth function $H_\epsilon(\phi)$ and $\delta_\epsilon(\phi)$ defined as

$$H_\epsilon(\phi) = \begin{cases} \frac{1}{2}\left(1 + \frac{x}{\epsilon} + \frac{1}{\pi} sin\left(\frac{\pi x}{\epsilon}\right)\right), & |x| \le \epsilon \\ 1, & x > \epsilon \\ 0, & x < -\epsilon \end{cases} \tag{16}$$

$$\delta_\epsilon(\phi) = \begin{cases} \frac{1}{2\epsilon}\left(1 + cos\left(\frac{\pi x}{\epsilon}\right)\right), & |x| \le \epsilon \\ 0, & |x| > \epsilon \end{cases} \tag{17}$$

where $\delta_\epsilon(\phi)$ is the derivative of $H_\epsilon(\phi)$. Through replacing $\delta(\phi)$, $H(\phi)$ by $\delta_\epsilon(\phi)$, $H_\epsilon(\phi)$ in formula (13), (14) and (15), we can obtain the evolution equations used in practice:

$$\begin{aligned} \frac{\partial \phi_1}{\partial t} = {} & [\lambda_{1,0}\delta_\epsilon(\phi_1) + \lambda_{1,k}\delta_\epsilon(\phi_1 - k)] div\left(g\frac{\nabla\phi_1}{|\nabla\phi_1|}\right) + \\ & \alpha_{1,0} g\delta_\epsilon(\phi_1) + \alpha_{1,k} g\delta_\epsilon(\phi_1 - k) + \gamma\delta_\epsilon(-\phi_1)H_\epsilon(\phi_2) \\ & + \mu_1\left[\nabla^2\phi_1 - div\left(\frac{\nabla\phi_1}{|\nabla\phi_1|}\right)\right] \end{aligned} \tag{18}$$

$$\begin{aligned} \frac{\partial \phi_2}{\partial t} = {} & -\delta_\epsilon(\phi_2)(\lambda_{2,1}e_1 - \lambda_{2,2}e_2) + \nu_2\delta_\epsilon(\phi_2) div\left(\frac{\nabla\phi_2}{|\nabla\phi_2|}\right) \\ & + \mu_2\left(\nabla^2\phi_2 - div\left(\frac{\nabla\phi_2}{|\nabla\phi_2|}\right)\right) + \gamma\delta_\epsilon(-\phi_2)H_\epsilon(\phi_1) \end{aligned} \tag{19}$$

And the calculation of f_1 and f_2 becomes

$$f_i(x) = \frac{K_\sigma * [M_i^\epsilon(\phi_2(x))I(x)]}{K_\sigma * M_i^\epsilon(\phi_2(x))}, i = 1, 2 \tag{20}$$

In our experiments, the parameters are set as follows. For the level set ϕ_1, we set $\lambda_{1,0} = 5$, $\lambda_{1,k} = 5$, $\alpha_{1,0} = -3.3$, $\alpha_{1,k} = -1.3$, $\mu_1 = 0.2$. Since in our experiments the level sets which take negative value inside the zero level set are used, we choose $\alpha_{1,0}$ and $\alpha_{1,k}$ as the negative value

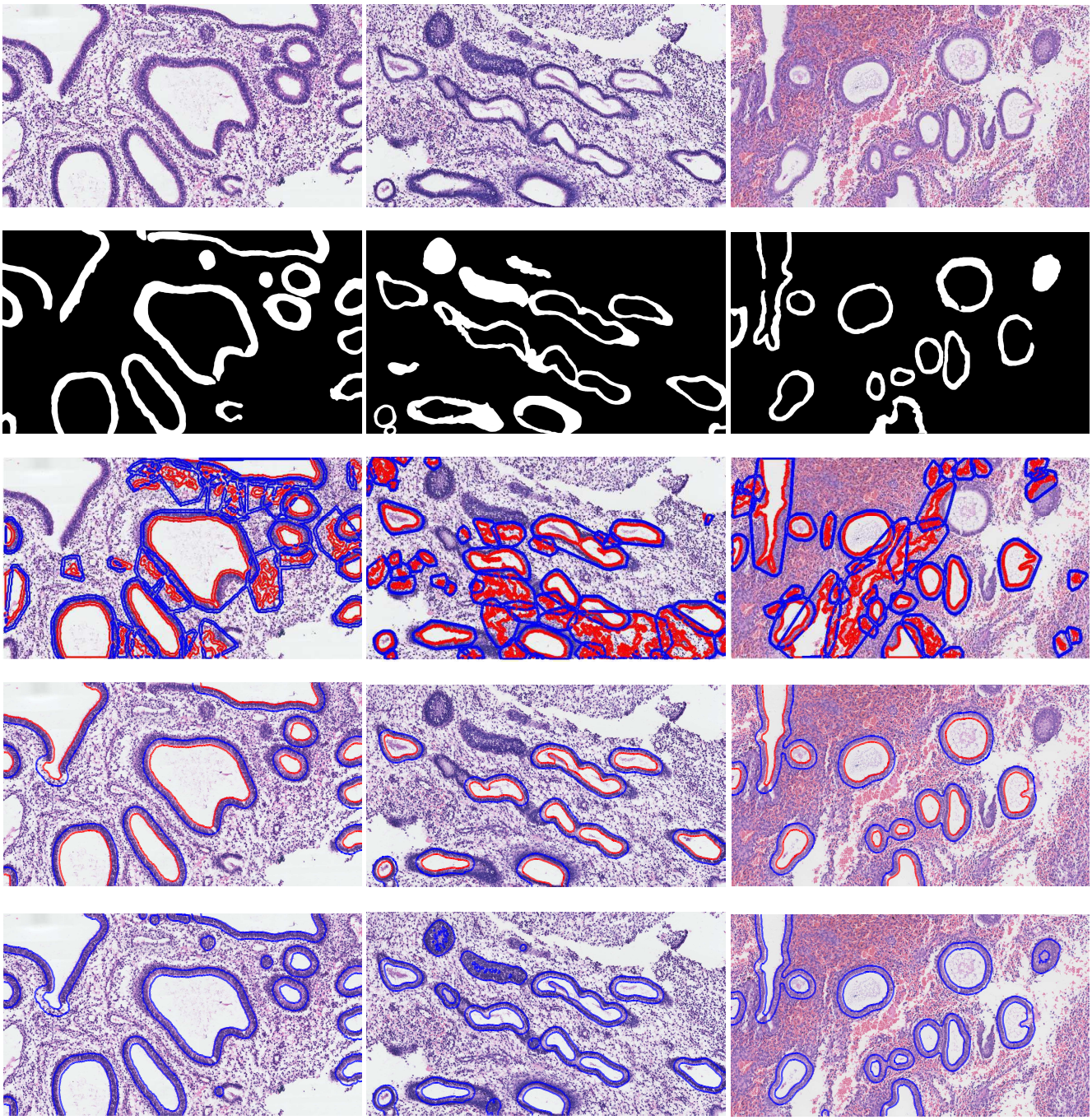

Figure 7. The experimental results of different segmentation methods. The three columns show different segmentation results of three different images. The first row is the original images. The second row is the ground truth. The third, fourth and fifth rows are the results of Nguyen et al. [9], the edge-based level set model using 0, k levels and our methods, respectively.

to let the initial contour expand. We can set the parameter k according to $k/d = s$, where d is the distance from 0 level contour to k level contour and s is the slope of the level set. Since the thickness of epithelial layers is similar for different images, we set $k = 6$ for the down-sampled images and $s = 1$ for level sets. As for the level set ϕ_2, we set $\lambda_{2,1} = 1.0,\ \lambda_{2,2} = 1.0,\ \nu_2 = 0.004 \times 255 \times 255$, and $\mu_2 = 1.5$.

4.3. Performance evaluation

We use Dice similarity coefficient (DSC) and Euler Distance (ED) between obtained contours and ground truth to

validate the segmentation accuracy of our proposed method. Given a set of regions G representing the ground truth and S representing the result of the segmentation method, DSC describes the similarity of G and S, which is defined as

$$DSC(G,S) = \frac{2 \times |G \cap S|}{|G| + |S|} \tag{21}$$

where $|*|$ is the area of region $*$. For the evaluation of the segmentation method, we calculate the DSC of obtained results and the ground truth. A higher value of DSC means a better performance. The DSC of our proposed method and the other method is shown in Fig. 8(a).

Given the contour c_s which is obtained by the segmentation method and c_g which is the contour of the ground truth, ED calculates the distance from c_s to c_g.

$$ED(c_s, c_g) = \frac{1}{2}\left(\sum_{i \in c_s} D(i, c_g) + \sum_{j \in c_g} D(c_s, j)\right) \tag{22}$$

where $D(i, c_g)$ represents the distance from the pixel i to the contour c_g, which is calculated as $D(i, c_g) = \min_{j \in c_g} d(i, j)$ and $D(c_s, j)$ is defined similarly. ED is more convenient to be used for evaluating the method which only obtains the contour. Since the contour may not be closed, it is difficult to obtain the corresponding regions and the DSC can not be calculated. We can see that the ED will be lower if the segmentation contours are more close to the ground truth. Meanwhile, the over segmentation and the under segmentation result in a higher ED (i.e., worse performance).

4.4. Experimental results and comparison

To validate the segmentation accuracy of the proposed approach, we compare our method with Nguyen et al. [9] and the edge-based level set model using 0, k levels. It is worth mentioning that the edge-based level set model using 0, k levels plays the same role as ϕ_1 in our proposed method. Through experimental comparison, we demonstrate the improvement of our model built by introducing two level sets.

Notice that the pre-processing can improve the computational speed and the segmentation accuracy of all three methods. For a fair comparison, we apply the pre-processing for all three methods. The segmentation results are shown in Fig. 7. It can be seen that both Nguyen et al. and the edge-based level set using 0, k levels can not deal with the glands without lumens, while our proposed method can obtain the boundary of glands without lumens. Notice that the Nguyen et al. also suffers from the interference of vessels.

For the quantitative evaluation, we use DSC and ED to evaluate the accuracy of the three methods. Due to the results of Nguyen et al. are contours which are not closed, we only compute DSC for our method and the edge-based level set model using 0, k levels. The DSC box plot is shown in Fig. 8(a). From the figure we can see that our method has a higher DSC value, because our method can obtain the glands without lumens by searching in the complementary part.

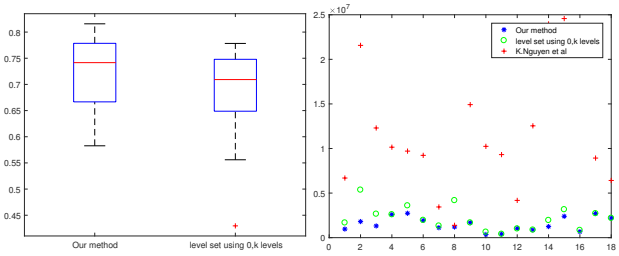

(a) Dice boxplot (b) ED of different methods for 18 images.

Figure 8. Quantitative evaluation of different methods.

ED is computed for all three methods. The computed value is shown in Fig. 8(b), where the x-axis represents 18 images and the y-axis represents the ED from the segmentation contours to the ground truth. The ED of our method, the edge-based level set model using 0, k levels and Nguyen et al. are shown in blue $*$, green $\circ$ and red $+$, respectively. From Fig. 8(b) we can see that our proposed approach obtains the contours which are most close to the ground truth for every image. The edge-based level set model using 0, k levels and Nguyen et al. cause under segmentation in several cases containing glands without lumens.

5. Conclusion

In this paper we propose a level set framework for gland segmentation in which two level sets based on edge-based and region-based models are used. In order to obtain both the glands with and without lumens, we propose to divide the whole image into the main part and the complementary part. The main part consists of the glands with lumens, which can be located and segmented by the edge-based level set. The complementary part contains mostly stromal nuclei and the possibly existed glands without lumens. The final result is the combination of obtained regions of these two level sets. The experimental results demonstrate that our method can deal with the images containing glands without lumens. Thus our method has a better performance.

References

[1] G. Aubert and P. Kornprobst. *Mathematical problems in image processing: partial differential equations and the calculus of variations*, volume 147. Springer Science & Business Media, 2006. 4

[2] H. Chen, X. Qi, L. Yu, and P.-A. Heng. Dcan: Deep contour-aware networks for accurate gland segmentation. In *Pro-*

ceedings of the IEEE conference on Computer Vision and Pattern Recognition, pages 2487–2496, 2016. 2

[3] C. Gunduz-Demir, M. Kandemir, A. B. Tosun, and C. Sokmensuer. Automatic segmentation of colon glands using object-graphs. *Medical image analysis*, 14(1):1–12, 2010. 2

[4] M. N. Gurcan, L. E. Boucheron, A. Can, A. Madabhushi, N. M. Rajpoot, and B. Yener. Histopathological image analysis: A review. *IEEE reviews in biomedical engineering*, 2:147–171, 2009. 1, 2, 6

[5] A. Janowczyk and A. Madabhushi. Deep learning for digital pathology image analysis: A comprehensive tutorial with selected use cases. *Journal of pathology informatics*, 7, 2016. 2

[6] C. Li, C.-Y. Kao, J. C. Gore, and Z. Ding. Minimization of region-scalable fitting energy for image segmentation. *IEEE transactions on image processing*, 17(10):1940–1949, 2008. 4

[7] C. Li, C. Xu, C. Gui, and M. D. Fox. Distance regularized level set evolution and its application to image segmentation. *IEEE Transactions on image processing*, 19(12):3243–3254, 2010. 3

[8] S. Naik, S. Doyle, S. Agner, A. Madabhushi, M. Feldman, and J. Tomaszewski. Automated gland and nuclei segmentation for grading of prostate and breast cancer histopathology. In *Biomedical Imaging: From Nano to Macro, 2008. ISBI 2008. 5th IEEE International Symposium on*, pages 284–287. IEEE, 2008. 2

[9] K. Nguyen, A. Sarkar, and A. K. Jain. Structure and context in prostatic gland segmentation and classification. In *International Conference on Medical Image Computing and Computer-Assisted Intervention*, pages 115–123. Springer, 2012. 2, 6, 7, 8

[10] A. Paul and D. P. Mukherjee. Gland segmentation from histology images using informative morphological scale space. In *Image Processing (ICIP), 2016 IEEE International Conference on*, pages 4121–4125. IEEE, 2016. 2